Article:
Zhang, ZQ (2015) Two-step calibration methods for miniature inertial and magnetic sensor units. IEEE Transactions on Industrial Electronics, 62 (6). pp. 3714-3723. ISSN: 0278-0046

https://doi.org/10.1109/TIE.2014.2375258

Two-Step Calibration Methods for Miniature Inertial and Magnetic Sensor Units

Zhi-Qiang Zhang

***Abstract*—Low-cost inertial/magnetic sensor units have been extensively used to determine sensor attitude information for a wide variety of applications, ranging from virtual reality, underwater vehicles, handheld navigation systems, to bio-motion analysis and biomedical applications. In order to achieve precise attitude reconstruction, appropriate sensor calibration procedures must be performed in advance to process sensor readings properly. In this paper, we are aiming to calibrate different error parameters, such as sensor sensitivity/scale factor error, offset/bias error, non-orthogonality error, mounting error, and also the soft iron and hard iron errors for magnetometer. Instead of estimating all these parameters individually, these errors are combined together as the combined bias and transformation matrix. Two-step approaches are proposed to determine the combined bias and transformation matrix separately. For the accelerometer and magnetometer, the combined bias is determined by finding an optimal ellipsoid that can best fit the sensor readings, and the transformation matrix is then derived through a two-step iterative algorithm by exploring the intrinsic relationship among sensor readings. For the gyroscope, the combined bias can be easily determined by placing the sensor node stationary. For the transformation matrix estimation, the intrinsic relationship among gyroscope readings is also again, and an unscented Kalman filter is employed to determine such matrix. The calibration methods are then applied to our sensor nodes, and the good performance of the orientation estimation has illustrated the effectiveness of the proposed sensor calibration methods.**

***Keywords*-Miniature Sensors, Calibration, Orientation/Attitude, Kalman Filter, Optimization**

I. Introduction

In the past decade, low-cost inertial/magnetic sensor units have been extensively used to determine sensor attitude information for a wide variety of applications, ranging from virtual reality, underwater vehicles, handheld navigation systems, to bio-motion analysis and biomedical applications [1] [2] [3] [4]. A typical inertial/magnetic sensor unit contains a triaxial accelerometer, a triaxial gyroscope, and a triaxial magnetometer, and these sensors are usually assembled together on a printed circuit board to form an inertial/magnetic measurement node. Thus far, extensive research has been performed on how to accurately determine attitude information from micro inertial/magnetic sensor measurements [5] [6]. Some researchers even moved beyond this and proposed to estimate the sensor displacement as well [7] [8] [9]. However, the achievable accuracy is highly dependent on the quality of the inertial/magnetic sensor unit measurements; therefore, appropriate sensor calibration procedures must be performed in advance to process sensor readings properly.

In general, the inaccurate sensor measurements are mainly caused by sensor sensitivity/scale factor error, offset/bias error, non-orthogonality error and mounting error. In addition, soft iron error and hard iron error may also contribute to the inaccuracy of the magnetometer measurements. Thus far, a large number of calibration methods, ranging from very simple procedures to very sophisticated ones using expensive equipment such as optical systems or robotic systems [10] [11] [12], have been proposed to determine some of these error parameters for the inertial/magnetic sensor unit. The basic idea of these methods is to construct a cost function and then to minimize it with respect to the unknown sensor error parameters using specific optimization methods. For example, Skog et al. [13] considered the scale factor error, offset/bias error and non-orthogonality error for inertial sensor calibration. A nonlinear cost function was constructed to describe the relationship between the squared magnitude of the input and the squared magnitude of the output, and the Newton-Raphson method was then applied to minimize the cost function. Based on the similar cost function, Li et al. [14] and Skaloud et al. [15] also presented their solutions for the optimization problem, and we also had the similar work presented in [16]. The underlying assumption for these methods is that the physical quantities and the corresponding raw sensor readings can be acquired simultaneously; however, such assumption may not be easy to satisfy in practice. Furthermore, all these methods only considered the inertial sensor calibration in the sensor frame, and the mounting misalignment error was ignored in their methods. Due to the difficulties of acquiring the magnetic field information and the existence of the magnetic soft iron error and hard iron error, the aforementioned inertial sensor calibration methods are not applicable to the magnetometer calibration. For this reason, a number of magnetometer calibration methods have been proposed to determine some of the error parameters. For instance, Renaudin et al. [17] elaborated a complete sensor error model, and then derived an adaptive least squares estimator which provided a consistent solution to the ellipsoid fitting problem. Based on the similar sensor error model, Vasconcelos et al. [18] formulated the calibration problem as the optimization of the sensor readings' likelihood, and proposed an iterative maximum likelihood estimator (MLE) for it. Wu et al. [19] further extended Vasconcelos's work and proposed to use particle swarm optimization (PSO) strategy

Manuscript received May 21, 2014; revised September 17, 2014; accepted for publication October 31, 2014.

The author is with the Department of Computing, Imperial College London, SW7 2AZ London, U. K. (e-mail: z.zhang@imperial.ac.uk).

and stretching technique together, which could help to prevent Vasconcelos's method from converging to a local maxima and preserve the global ones. Springmann et al. [20] and Pang et al. [21] also presented similar work for magnetometer calibration. Unfortunately, all these magnetometer calibration methods implicitly assumed that some magnetic field information could be acquired in advance, which might not be possible in practice. Moreover, similar to the inertial sensor calibration, they also ignored the potential mounting misalignment error, which is critical to integrate the magnetometer together with the inertial sensors.

The motivation of the paper is to tackle all the error parameters, including sensor sensitivity/scale factor error, offset/bias error, non-orthogonality error, mounting error, and also the soft iron and hard iron errors for magnetometer, and provide a unified framework for the micro inertial/magnetic sensor unit calibration without using any extra instrument to measure the magnetic field. Since the main purpose of the sensor calibration is to convert the raw sensor readings to sensor measurements in metric unit, there is no need to estimate all these parameters individually; therefore, we combine these errors together as the combined bias and transformation matrix. Two-step approaches are proposed to determine the combined bias and transformation matrix separately. For the accelerometer and magnetometer, the combined bias is determined by finding an optimal ellipsoid that can best fit the sensor readings, and the transformation matrix is derived through a two-step iterative algorithm by exploring the intrinsic relationship among sensor readings. For the gyroscope, the combined bias can be easily determined by placing the sensor node stationary. For the transformation matrix estimation, the intrinsic relationship among sensor readings is explored again, and an unscented Kalman filter is employed to determine such matrix. The calibration methods are then applied to our sensor nodes, and the good performance of the orientation estimation has illustrated the effectiveness of the proposed sensor calibration methods.

The rest of the paper is organized as follows. The proposed sensor calibration procedures, including the unified sensor model, the accelerometer and magnetometer calibration, and the gyroscope calibration are given in section II. Experimental results and conclusions are provided in sections III and IV, respectively.

II. Our method

A. Unified sensor model

For the inertial sensors, the main sources of the sensor error include bias, scale factor, non-orthogonality and mounting misalignment, thus we can have the following model to compensate for such errors:

$$u_k = R_k T_k S_k (y_k - b_k) \tag{1}$$

where index k represents the sensor type (i.e., *a, g* for accelerometer or gyroscope respectively), u_k is the measured physical quantities in metric unit, and the y_k is raw sensor readings. b_k is the bias vector, S_k is the scale factor matrix, T_k is the Gram-Schmidt orthogonalization matrix, and R_k is the rotation matrix to correct the mounting error. Here, u_k, y_k and b_k are 3×1 vectors, while R_k, T_k and S_k are 3×3 matrices. Since the main purpose is to find an accurate u_k for any sensor reading y_k, there is no need to estimate the R_k, T_k, S_k and b_k separately. Therefore, we can define the combined bias $B_k = b_k$ and transformation matrix $H_k = R_k T_k S_k$, and then estimate B_k and H_k instead to ease the calibration process. Similarly, for the magnetometers, in addition to these sensor errors, there are also soft iron error and hard iron error, so we can have the following model considering all the errors [22]:

$$\begin{aligned} u_m =& R_m T_m S_m (A_{si} y_m - b_{hi} - b_m) \\ =& R_m T_m S_m A_{si} \left(y_m - A_{si}^{-1} (b_{hi} + b_m) \right). \end{aligned} \tag{2}$$

where R_m, T_m, S_m and b_m correspond to the four different sensor errors, while A_{si} and b_{hi} are associated with soft iron error and hard iron error, respectively. Similarly, u_m, y_m, b_{hi} and b_m are 3×1 vectors, while R_m, T_m, S_m and A_{si} are 3×3 matrices. We can then also define

$$B_m = A_{si}^{-1} (b_{hi} + b_m) \tag{3}$$

and

$$H_m = R_m T_m S_m A_{si} \tag{4}$$

thus a unified sensor model for inertial sensor and magnetometer can be written as:

$$u_k = H_k (y_k - B_k). \tag{5}$$

For simplicity, we used index k again to represent the sensor type (*a, g, m* for accelerometer, gyroscope or magnetometer respectively). In the above equation, B_k, a 3×1 vector, is regarded the combined bias, while H_k, a 3×3 matrix, is taken as the transformation matrix. The other advantage of amalgamating these error parameters together as the combined bias and transformation matrix is that they can also take the other unmodeled linear time invariant errors and distortions into consideration. Thus, the purpose of the sensor calibration is to estimate the value:

$$\zeta = \{H_k,\ B_k\}^T \tag{6}$$

given J sensor raw readings y_k^j, where $j = 1, 2, \cdots, J$, and the magnitude of the earth magnetic field M and gravity G. The estimation of ζ can be written as:

$$\hat{\zeta} = \underset{\zeta}{\operatorname{argmin}} \{L(\zeta)\} \tag{7}$$

where

$$L(\zeta) = \sum_{j=1}^{J} \left\| u_k^j - H_k (y_k^j - B_k) \right\|^2 \tag{8}$$

subject to

$$|u_a^j| = G \tag{9}$$

and

$$|u_m^j| = M. \tag{10}$$

Here, $|\cdot|$ and $\|\cdot\|$ are the magnitude and Frobenius norm operators, respectively, and j is the index of different orientation or rotation that the sensor node is set to. Due to the nonlinearity of (8), it is difficult to find a globally optimized solution for

ζ in practice. In this paper, we propose two-step parameter estimation schemes to simplify the optimization process, 1) estimate the combined bias B_k; 2) estimate the transformation matrix H_k.

B. Accelerometer/Magnetometer Calibration

For accelerometer and magnetometer, the magnitude of the measured physical quantity u_a^j or u_m^j are constant and independent of the sensor node orientation; therefore, the calibration methods for the accelerometer and magnetometer are the same. In this section, we take the accelerometer as the example to introduce the two step calibration method. The same method can also be applied for magnetometer calibration.

1) Combined Bias B_a Estimation: For the accelerometer, the sensor model can be rewritten as:

$$u_a^j = H_a(y_a^j - B_a). \tag{11}$$

For any accelerometer reading y_a^j, the magnitude of u_a^j is equal to the magnitude of gravity, so we can have:

$$|H_a(y_a^j - B_a)| = |u_a^j| = G. \tag{12}$$

By expanding the above equation, we can get:

$$\left(y_a^j - B_a\right)^T \cdot (H_a)^T \cdot H_a \cdot \left(y_a^j - B_a\right) = G^2. \tag{13}$$

Thus we can normalize the above equation as:

$$\left(y_a^j - B_a\right)^T \cdot \left(\frac{H_a}{G}\right)^T \cdot \frac{H_a}{G} \cdot \left(y_a^j - B_a\right) = 1. \tag{14}$$

Expanding this equation we obtain

$$\left(y_a^j\right)^T \cdot \Sigma \cdot y_a^j - \left(y_a^j\right)^T \cdot \Gamma + \Upsilon = 0 \tag{15}$$

where

$$\begin{aligned} \Sigma &= \left(\frac{H_a}{G}\right)^T \frac{H_a}{G} \\ \Gamma &= 2\Sigma \cdot B_a \\ \Upsilon &= (B_a)^T \cdot \Sigma \cdot B_a - 1. \end{aligned} \tag{16}$$

This equation is the algebraic equation of an ellipsoid, and the calibration problem now becomes finding an arbitrarily oriented ellipsoid which fits the J sensor readings $y_a^1, y_a^2 \cdots y_a^J$ best. There is abundant literature addressing this problem [23] [24] [25]. For this study, the least squares ellipsoid fitting method proposed in [26] is used, and the values of Σ, Γ and Υ can be then obtained. Denote the estimates for Σ and Γ as $\hat{\Sigma}$, $\hat{\Gamma}$, we can have estimate for B_a as:

$$\hat{B}_a = \frac{1}{2}\left(\hat{\Sigma}\right)^{-1}\hat{\Gamma} \tag{17}$$

and H_a has the following property:

$$(H_a)^T \cdot H_a = G^2\hat{\Sigma}. \tag{18}$$

Since $\hat{\Sigma}$ is a positive definite matrix, an eigen-decomposition can be applied:

$$\hat{\Sigma} = \Lambda D \Lambda^T \tag{19}$$

where Λ corresponds to the eigenvectors of $\hat{\Sigma}$, and D is the diagonal matrix containing the eigenvalues. Thus we can define another matrix K as

$$K = G\Lambda\sqrt{D}\Lambda^T \tag{20}$$

satisfying

$$\begin{aligned} K^T K =& G\Lambda\sqrt{D}\Lambda^T G S \sqrt{D}\Lambda^T \\ =& G^2 \Lambda D \Lambda^T \\ =& G^2\hat{\Sigma}. \end{aligned} \tag{21}$$

However, given any rotational matrix Ω, we can also have

$$\begin{aligned} (\Omega K)^T \Omega K =& G S \sqrt{D}\Lambda^T \Omega^T \Omega G \Lambda \sqrt{D}\Lambda^T \\ =& G^2 \Lambda D \Lambda^T \\ =& G^2\hat{\Sigma}. \end{aligned} \tag{22}$$

Therefore, the factorization $(H_a)^T H_a = G^2\hat{\Sigma}$ is not unique, and H_a can be any matrix in the form of ΩK, so it is impossible to acquire the exact transformation matrix H_a through the ellipsoid fitting, while the combined bias B_a can be estimated as $\hat{B}_a$. In the next section, we will discuss how to determine the transformation matrix by exploring the intrinsic relationships among the sensor readings.

2) Transformation Matrix H_a Estimation: In the previous section, any two sensor readings y_a^i and $y_a^j (i = 1, 2 \cdots J$ and $i \neq j)$ are used independently. However, both indexes i and j indicate the orientations or rotations that the sensor calibration unit is set to; therefore, we can also get the orientation difference R_j^i between the i^{th} orientation and j^{th} orientation during the calibration process. Thus we can have:

$$u_a^i = H_a \cdot \left(y_a^i - B_a\right) \tag{23}$$

and

$$u_a^j = R_j^i u_a^i = H_a \cdot \left(y_a^j - B_a\right). \tag{24}$$

Denote $R_i^i = I_3$ as the identity matrix of order 3, the estimate of H_a can be written as:

$$\{\hat{H}_a, \hat{u_a^i}\} = \underset{H_a, u_a^i}{\operatorname{argmin}} \left\{ \sum_{j=1}^{J} \left\| R_j^i u_a^i - H_a\left(y_a^j - B_a\right) \right\|^2 \right\} \tag{25}$$

subject to

$$|u_a^i| = G \tag{26}$$

given sensor readings $y_a^1, y_a^2 \cdots y_a^J$ and orientation differences $R_1^i, R_2^i \cdots R_J^i$. There are a number of algorithms, such as interior point algorithm [27], active set algorithm [28], sequential quadratic programming (SQP) algorithm [29], have been proposed to solve the above constrained minimization problem, but these methods tend to calculate the Jacobian matrix and Hessian matrix, which are computationally expensive. In this paper, we propose a simple two step iteration method to solve the above constrained optimization problem.

Lemma 1: Denote a $3 \times J$ matrix Y_a as:

$$Y_a = \left[y_a^1 - \hat{B}_a, y_a^2 - \hat{B}_a, \cdots, y_a^J - \hat{B}_a\right] \tag{27}$$

and a $3J \times 3$ matrix $\mathcal{R}$ as

$$\mathcal{R} = \begin{bmatrix} R_1^i \\ R_2^i \\ \vdots \\ R_J^i \end{bmatrix} \tag{28}$$

H_a and u_a^i thus satisfy:

$$\begin{aligned} C2M\left(\mathcal{R}u_a^i\right) &= H_a Y_a \\ \mathcal{R}u_a^i &= M2C\left(H_a Y_a\right) \end{aligned} \tag{29}$$

where $C2M(\cdot)$ is to convert a $3J \times 1$ vector to a $3 \times J$ matrix while $M2C(\cdot)$ is the inverse operation of $C2M(\cdot)$, converting a $3 \times J$ matrix to a $3J \times 1$ vector (refer to the Appendix for detailed definition).

Given an initial vector $u_{a,0}^i$, the H_a and u_a^i can be estimated as:

1. set index $k = 1$;
2. calculate $H_{a,k}$ as:
$$H_{a,k} = C2M\left(\mathcal{R}u_{a,k-1}^i\right) \cdot Y_a^+ \tag{30}$$
where $(\cdot)^+$ is the pseudo-inverse operator.
3. calculate $u_{a,k}^i$ as
$$u_{a,k}^i = \mathcal{R}^+ \cdot M2C(H_{a,k}Y_a). \tag{31}$$
4. set $k = k + 1$ and repeat steps $2 - 4$ until H_a and u_a^i converge.
5. re-scale the magnitudes and set the H_a and u_a^i estimates as
$$\begin{aligned} \hat{u}_a^i &= \frac{G}{|u_{a,k}^i|} u_{a,k}^i \\ \hat{H}_a &= \frac{G}{|u_{a,k}^i|} H_{a,k}. \end{aligned} \tag{32}$$

The purpose of the equation (25) is to minimize

$$\left\| C2M(\mathcal{R}u_a^i) - H_a Y_a \right\| \tag{33}$$

or

$$\left\| \mathcal{R}u_a^i - M2C(H_a Y_a) \right\|. \tag{34}$$

To make sure H_a and u_a^i converge, we need to prove in each iteration that:

$$\left\| C2M(\mathcal{R}u_{a,k}^i) - H_{a,k+1}Y_a \right\| \leqslant \left\| C2M(\mathcal{R}u_{a,k}^i) - H_{a,k}Y_a \right\| \tag{35}$$

and

$$\left\| \mathcal{R}u_{a,k}^i - M2C(H_{a,k}Y_a) \right\| \leqslant \left\| \mathcal{R}u_{a,k-1}^i - M2C(H_{a,k}Y_a) \right\|. \tag{36}$$

The proofs for equation (35) and (36) are given in the Appendix at the end of this paper.

C. Gyroscope Calibration

Similar to accelerometer/magnetometer calibration, we also estimate the gyroscope combined bias B_g and transformation matrix H_g separately.

1) Combined Bias B_g Estimation: Similar the accelerometer/magnetometer calibration, there is also some constant magnitude information which can be used for gyroscope combined bias estimation. When the gyroscope is stationary, the gyroscope measurements should be 0. Therefore, we can place the sensor node at J different orientations and remain stationary, which means that $u_g^j = 0, j = 1, 2 \cdots, J$. Denote the corresponding gyroscope reading as y_g^j, we can then have:

$$H_g \cdot \left(y_g^j - B_g\right) = 0, \quad j = 1 \cdots, J. \tag{37}$$

The above equation can be written in the matrix format as:

$$H_g \cdot (Y_g - \mathbb{B}_g) = 0 \tag{38}$$

where

$$Y_g = \left[y_g^1, y_g^2 \cdots, y_g^J\right] \tag{39}$$

and $\mathbb{B}_g$ is a $3 \times J$ matrix, and every column is set to B_g. Since H_g is a full rank matrix, we can then have

$$Y_g - \mathbb{B}_g = 0. \tag{40}$$

By taking sensor noise into account, we set bias B_g estimate as the mean value:

$$\hat{B}_g = \frac{\sum_{j=1}^{J_1} y_g^j}{J}. \tag{41}$$

2) Transformation Matrix H_g Estimation: During our calibration process, the time is usually less than 2s when we rotate the sensor node from orientation j to $j + 1$. In such a short time period, the gyroscope measurements can be integrated to produce accurate orientation estimation. Since we already know the orientation difference R_j^{j+1} between them, we can have:

$$Q(R_j^{j+1}) = Int(y_g^{j,1:N_j}, H_g) \tag{42}$$

where $Q(R_j^{j+1})$ is the corresponding quaternion representation of the rotation matrix R_j^{j+1} [3], $y_g^{j,1:N_j} = \{y_g^{j,1}, y_g^{j,2}, \cdots, y_g^{j,N_j}\}$ are the gyroscope readings during the period rotating the sensor from the orientation j to $j+1$, N_j is the number of the sensor readings during this period, and Int is the gyroscope integration operator (refer to the Appendix for detailed definition). Thus, the estimation of H_g can be written as:

$$\hat{H}_g = \underset{H_g}{\operatorname{argmin}} \left\{ \sum_{j=1}^{J-1} \left\| Q(R_j^{j+1}) - Int(y_g^{j,1:N_j}, H_g) \right\|^2 \right\}. \tag{43}$$

Similar to the optimization problem in equation (25), several algorithms, such as Quasi-Newton method [30] and Nelder-Mead method [31], have been proposed to solve such unconstrained minimization problem, but these methods also have to calculate the Jacobian matrix and Hessian matrix, which are computationally expensive. In this paper, we propose a simple Kalman filter based method to solve the above unconstrained optimization problem. Thus, the process model for the Kalman filter can be written as:

$$X_k = X_{k-1} + v \tag{44}$$

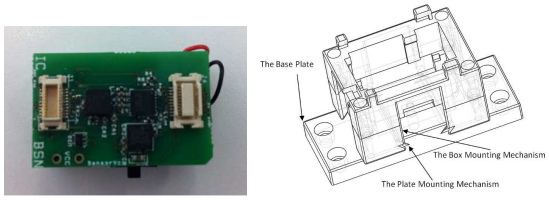

(a) (b)

Figure 1. The BSN hardware platform used for this study. (a) BSN Sensor Node and its stackable sensor daughter boards. (b) The bespoke housing for the BSN Sensor Node.

Figure 2. The BTS SMART-D system used for this study and the BSN node mounted with reflective markers for orientation accuracy evaluation.

X_k is the unfolded 9×1 state vector from H_g, v is the zero mean process noise with covariance R_v. In our implementation, we set R_v to a diagonal matrix with all its main diagonal entries as 10^{-1} empirically. The measurement model can then be written as:

$$\begin{bmatrix} Q(R_1^2) \\ Q(R_2^3) \\ \vdots \\ Q(R_{J-1}^J) \end{bmatrix} = \begin{bmatrix} Int(y_g^{1,1:N_1}, H_g) \\ Int(y_g^{2,1:N_2}, H_g) \\ \vdots \\ Int(y_g^{J-1,1:N_{J-1}}, H_g) \end{bmatrix} + w \quad (45)$$

where w is the zero mean measurement noise with covariance R_w. As given in the equation (42), the left-hand side of the above equation should be equal to the first item of the right-hand side of the equation in theory, which means that the measurement noise w is 0. In our implementation, we set R_w to a diagonal matrix with all its main diagonal entries as 10^{-7} empirically. Because of the nonlinearity of measurement model, the Unscented Kalman Filter (UKF) is employed in this paper. The detailed UKF equations can be found in [1] [32].

III. Experimental and Simulation Results

It is quite challenging to acquire the true-values of error parameters for an inertial/magnetic sensor unit; therefore, detailed simulation studies were carried out to evaluate the performance of the proposed two step sensor calibration methods. The simulation study was based on the Monte Carlo simulation, which was carried out in a workstation with 3.40 GHz Intel Core i7 processor and 16G RAM. Laboratory experiments were also conducted in this paper, and we used the Body Sensor Network (BSN) platform [33] developed by our lab, which consists of three stackable daughter boards: the sensor board, the main processor board, and the battery board. They are connected via a stackable connector design as shown in Fig. 1(a). Each BSN node used is equipped with an Analog Devices ADXL330 [34] for 3D acceleration measurement, an InvenSense ITG-3200 digital gyroscope [35] for 3D angular velocity measurement, and a Honeywell HMC5843 [36] for 3D magnetic field measurement. In order to calibrate the BSN node, a bespoke housing for the BSN node is designed as shown in Fig. 1(b). Since it is quite challenging to acquire the ground-truth of the calibration parameters, we thus used the BSN node for attitude estimation after applying the proposed calibration methods to our sensor node, and compared the estimated attitude to reference measurements provided by an optical motion tracking system BTS SMART-D [37]. The BTS system used in our experiment consisted of 9 cameras installed on the ceiling as shown in Fig. 2. By capturing the positions of the 3 reflective markers on the rigid body that the BSN housing is attached to, an error less than 0.267mm on a volume of $2.95 \times 1.65 \times 3.08m$ was achieved by the BTS system.

A. Accelerometer/Magnetometer Calibration Performance Evaluation

In this step of the evaluation process, as the calibration procedures of the accelerometer and magnetometer are the same, we only present the simulation results for the accelerometer here. In the simulation, the estimation of the accelerometer combined bias B_a, transformation matrix H_a and reference acceleration vector u_a^i were studied when the sensor node was rotated into randomly selected 20 different orientations. However, a zero mean Gaussian distributed error with variance $0.1m^2/s$ was added to the sensor raw reading y_a to reflect sensor noise. In our simulation, the values of B_a, u_a^i and H_a are randomly set to:

$$B_a = [2429, 2318, 2368]^T$$

$$u_a^i = [2.6191601, 5.2383203, 7.8574805]^T$$

and

$$H_a = \begin{bmatrix} 0.0209850 & -0.0023786 & 0.0033562 \\ 0 & 0.0237864 & 0.0022374 \\ 0.0020985 & 0.0023786 & -0.0223744 \end{bmatrix}.$$

The simulation results for u_a^i and H_a are given in Fig. 3 and Fig. 4 respectively. We also applied the Matlab build-in SQP algorithm to optimize the constrained problem in equation (25) for comparison purpose, and the results derived from the SQP algorithm are also shown in the Fig. 3 and Fig. 4. As we can see from the figures, it is very clear that our proposed iterative method is relatively faster to converge. After about 8 iterations, the estimations for u_a^i and H_a are already very close to their respective ground-truth values, and the estimation errors are less than 1%. Although the optimization method can also converge to the ground-truth of u_a^i and H_a, convergence speed is much slower and it needs more than 15 iterations to achieve less than 1% error. We also noticed that the optimization method took about 1.5 seconds to complete all the iterations, while our method only took less than 0.05 second in our simulation. In fact, the SQP algorithm involves

Table I
ITERATIVE RESULTS OVER 1000 SIMULATIONS (SHOWN AS MEAN±STD)

	$\|H_a - \hat{H}_a\|$		$\|u_a^i - \hat{u}_a^i\|$	
	Optimization	Our	Optimization	Our
Iteration 2	2.5249±0.2518	0.1701±0.0965	11.8281±0.0256	1.3178±0.7496
Iteration 5	6.8363±2.4015	0.0586±0.0338	36.5101±14.1615	0.4349±0.2572
Iteration 10	6.2825±2.3289	0.0212±0.0066	36.1387±13.0760	0.0502±0.0203
Iteration 15	1.7143±1.8538	0.0149±0.0022	9.0593±11.0958	0.0118±0.0087
Iteration 20	0.0678±0.0847	0.0149±0.0022	0.3664±0.4672	0.0118±0.0087
Iteration 30	0.0147±0.0023	0.0149±0.0022	0.0161±0.0085	0.0118±0.0087
Iteration 50	0.0147±0.0023	0.0149±0.0022	0.0161±0.0085	0.0118±0.0087

sophisticated Hessian and Jacobian matrix operations, which are very computationally expensive. However, our proposed method only requires some basic matrix operations, such as multiplication and inverse, which therefore make our method much more efficient than the traditional optimization method.

The simulation was repeated for another 1000 times, and statistical results for u_a^i and H_a are given in Table I. It can be seen that the proposed iterative method converges after 15 iterations with negligible errors ($< 0.1\%$). Meanwhile, the error histogram of the combined bias B_a over the 1000 simulations is shown in the Fig 5. In the figure, over 93% of the estimated combined bias has smaller error than 0.1%. We also noticed that the maximum estimation error for the combined bias is 0.25%, which is small and imperceptible. In conclusion, the above analysis has shown that the proposed accelerometer calibration method can estimate the accelerometer sensor model parameters accurately.

B. Gyroscope Calibration Performance Evaluation

For the second simulation, we evaluated the gyroscope sensor model parameters estimation when we randomly rotate the the sensor to 10 predefined orientations. A zero mean

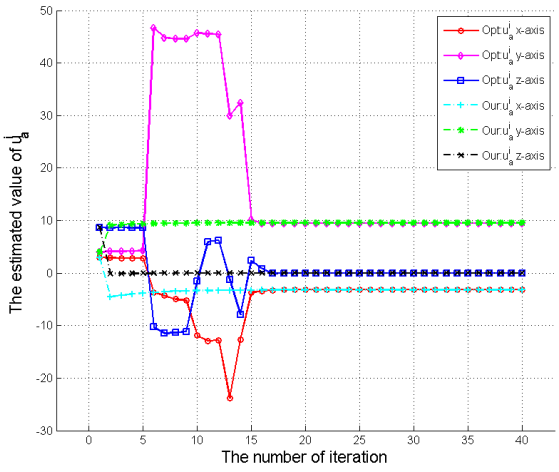

Figure 3. Estimation results for u_a^i, showing that the estimation value converges after 10 iterations using the proposed method while the optimization method needs 16 iterations.

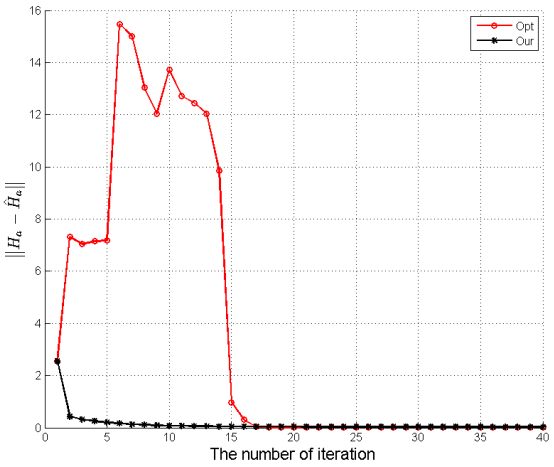

Figure 4. Estimation results for matrix H_a, showing that after 10 iterations, the Frobenius norm $\|H_a - \hat{H}_a\|$ converges to 0, i.e., $H_a = \hat{H}_a$.

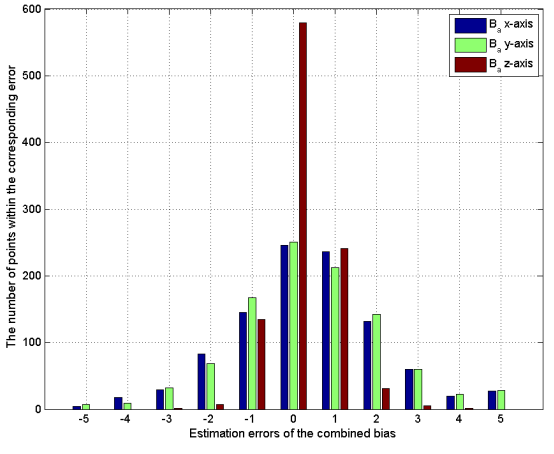

Figure 5. Statistic results for combined bias B_a, showing that the estimation errors for all of simulation are very small.

Gaussian distributed error with variance 0.05rad/s was added to the sensor readings y_g to simulate sensor noise. In this simulation, we only considered the transformation matrix H_g, and its estimation result is given in the Fig. 6. Similar to

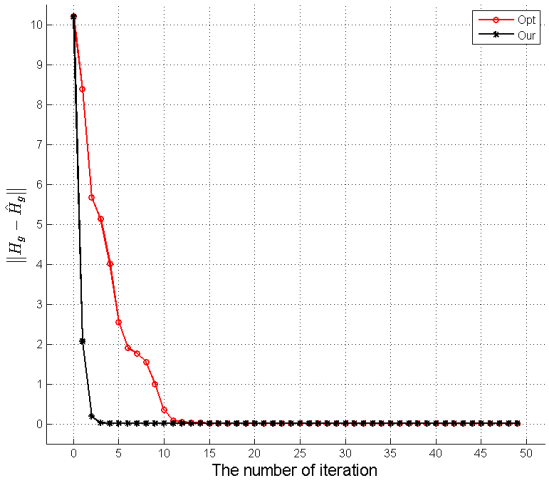

Figure 6. Estimation results for matrix H_g, showing that after 6 iterations, the Frobenius norm $\left\|H_g - \hat{H}_g\right\|$ converges to 0, i.e., $H_a = \hat{H}_g$.

Table II
ITERATIVE RESULTS OVER 1000 SIMULATIONS (SHOWN AS MEAN±STD)

	$\|H_g - \hat{H}_g\|$	
	Optimization	Our
Iteration 2	3.9872±0.4096	1.1261±0.6539
Iteration 5	1.8707±0.9048	0.0058±0.0043
Iteration 10	0.4532±0.6153	0.0045±0.0022
Iteration 20	0.0068±0.0121	0.0045±0.0022
Iteration 40	0.0045±0.0022	0.0045±0.0022
Iteration 50	0.0045±0.0022	0.0045±0.0022

the first simulation, we also implemented the trust region algorithm to optimize the unconstrained problem in equation (43), and the results for the trust region method are also shown in the Fig. 6. The second simulation was repeated for 1000 times, and statistical results for H_g is given in Table II. As we can see from the figure and table, both our method and the trust region can converge to the ground-truth of H_g, but the converge speed of our method is much faster than that of the trust region method. In general, our method only requires 10 iterations to get accurate estimation of H_g, while the trust region method needs about 40 iterations. Therefore, we can conclude that the proposed gyroscope calibration method can estimate the transformation matrix H_g accurately and efficiently.

It should be noted, however, we didn't evaluate the performance of the gyroscope combined bias estimation method yet since it is too simple to simulate. Therefore, in the next part of our evaluation, we will evaluate all the calibration methods together and show how the calibration methods can help to improve the attitude estimation accuracy significantly.

C. BSN Calibration Results

We then applied the proposed sensor calibration method to our BSN node. The sensor node was rotated to different orientations to evaluate the reproducibility of the proposed method. To make sure the magnetic distortion and local magnetic field are constant for different orientations, the sensor node was kept in a small area with ignorable translational movement when rotating the sensor node. Five data sets have been acquired, and in each data set, the sensor node was randomly placed at 10-20 different orientations. At each orientation, the sensor node was put on the table stationery to make sure the accelerometer only sense the gravity. At least 5s of data were collected for each orientation. Instead of using all the raw sensor readings for each orientation, only the mean value of these readings was used to increase the signal-to-noise ratio (SNR) for sensor model parameter determination. Fig. 7 takes the accelerometer for example and shows the estimation results for the combined bias B_a and the transformation matrix H_a. As we can see from the figures, both the combined bias and transformation matrix estimation results are similar for all the trials performed, and the deviations are small compared to the mean values. The consistency among all the five trials indicates the good repeatability of the proposed method. It is also worth mentioning that the estimation results for the gyroscope and magnetometer are also consistent among the

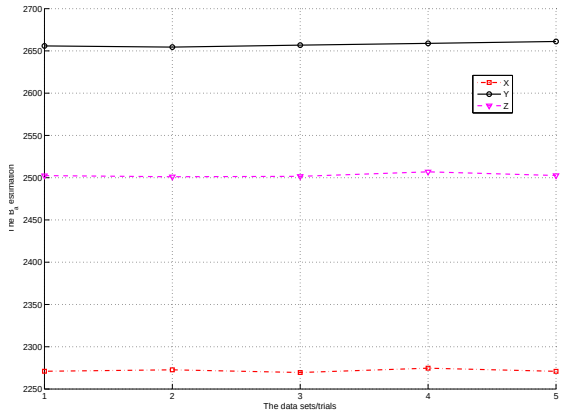

(a) Combined Bias

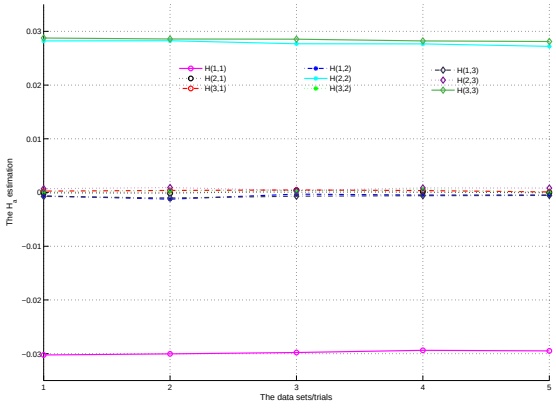

(b) Transformation Matrix

Figure 7. The accelerometer calibration results for the BSN sensor node. During the experiments, the same calibration method was repeated 5 times on the same sensor node. Although there is no ground-truth for the combined bias B_a and transformation matrix H_a, the estimation results have shown good consistency, which illustrates the robustness of our proposed method.

Table III
THE RMS, MEAN, SD AND CORRELATION COEFFICIENTS OF THE ESTIMATED ATTITUDE COMPARED TO THE BTS OPTICAL SYSTEM.

	Optimization Calibration		Our Calibration		Sensor Frame Calibration Only	
	RMS (Mean,SD)	Correlation Coefficient	RMS (Mean,SD)	Correlation Coefficient	RMS (Mean,SD)	Correlation Coefficient
Roll	0.0041 (0.0010±0.0040)	0.9997	0.0041 (0.0010±0.0040)	0.9997	0.0631 (-0.0157±0.0611)	0.9948
Pitch	0.0039 (0.0015±0.0077)	0.9998	0.0039 (0.0011±0.0076)	0.9998	0.0411 (-0.0130±0.0381)	0.9969
Yaw	0.0072 (0.0003±0.0072)	0.9998	0.0073 (0.0003±0.0072)	0.9998	0.0454 (0.0214±0.0398)	0.9953

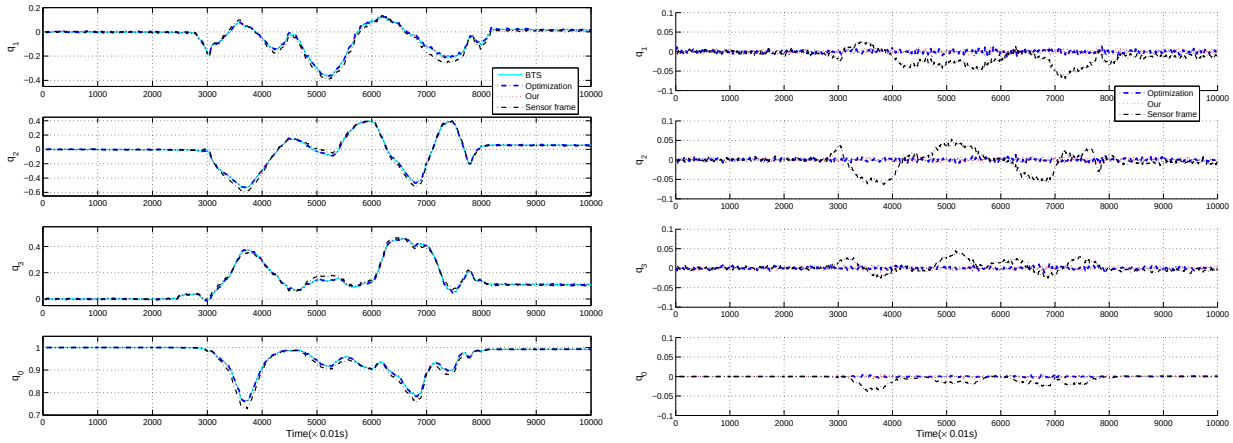

(a) Orientation estimation in quaternion

(b) Quaternion differences compared to BTS measurements

Figure 8. The orientation estimation results in quaternion compared to the BTS measurements. (a) the orientation estimation in quaternion, (b) the quaternion differences compared to BTS measurements.

five trials. Although there is no ground-truth for the combined bias and transformation matrix for the BSN sensor node, the consistency of the data illustrates the robustness of our proposed method.

After applying the calibration method to our BSN sensor nodes, we then fused the sensor measurements for attitude estimation using the method presented in [38]. We then compared the sensor based attitude estimation result with the reference measurement from the BTS optical motion tracker quantitatively. In our experiment, the BSN sensor node was placed on a rigid body affixed and rotated arbitrarily. Fig. 8 shows the orientation estimation results by using our proposed method compared to the ground-truth measurements from the optical motion tracking system BTS SMART-D. To better illustrate the orientation estimation accuracy, the quaternion differences compared to BTS measurements are also provided in the figure. It is evident that the proposed sensor calibration can estimate the BSN sensor model parameters accurately, and provide accurate sensor orientation estimation. We also noticed that although the converge speeds of optimization based methods are slower than our proposed iterative method, they can also provide accurate sensor orientation estimation. To further illustrate the strength of the proposed sensor calibration methods, we also implemented the sensor calibration methods which ignored the mounting error [13] [16], and the corresponding sensor orientation estimation results are also shown in the Fig. 8. It is obvious that there are significant improvements after taking the mounting error calibration into consideration. This is mainly because there are small errors among the coordinate systems of accelerometer, gyroscope and magnetometer, and such errors compromised the final orientation estimation accuracy. The quantitative comparison results between the BTS system and BSN sensor platform are shown in Table III. From the results derived, it is evident that the proposed method significantly reduces the root mean square (RMS) errors. There is also an excellent correlation between the calibrated result with that of the BTS system.

The above analyses have shown that the proposed inertial and magnetometer calibration methods can significantly improve the attitude estimation accuracy, which indicates that the calibration method can estimate the underlying sensor model parameters accurately. Based on the derived sensor model, the sensor readings can be converted to physical quantities in metric units for accurate attitude estimation.

IV. CONCLUSION AND FUTURE WORK

In conclusion, we have presented a unified calibration framework to determine different error parameters, such as sensor sensitivity/scale factor error, offset/bias error, non-orthogonality error, mounting error, and also the soft iron

error and hard iron error for magnetometer. We combined these error parameters together as the combined bias and transformation matrix, and two-step approaches were proposed to determine the combined bias and transformation matrix separately. The calibration method was applied to the BSN sensor node to acquire accurate acceleration, angular rate and magnetic field measurements, which could be fused by a quaternion-based linear Kalman filter to accurately derive the attitude information. The experimental results show that more accurate orientation information can be derived after effective sensor calibration. It is expected that the method can be used for a range of motion estimation applications including robotic navigation and human biomotion analysis.

In this paper, the temperature related sensor drift has not been addressed yet. Although this can be addressed by periodic re-calibration, it may present difficulties for practical applications. Therefore, further work is required for continuous self-calibration with consideration of different temporal characteristics of the sensors combined with the use of temperature controlled casing designs to minimise these errors. It is also possible to model and incorporate temperature related drift characteristics as the prior combined with real-time temperature monitoring to cater for these changes.

APPENDIX

A. Definition of $C2M$ and $M2C$

Given any $3 \times J$ matrix

$$M = \begin{bmatrix} m_1 & m_4 & \cdots & m_{3J-2} \\ m_2 & m_5 & \cdots & m_{3J-1} \\ m_3 & m_6 & \cdots & m_{3J} \end{bmatrix} \tag{46}$$

the $M2C$ operator can be defined as:

$$M2C(M) = [m_1, m_2, m_3, \cdots, m_{3J}]^T \tag{47}$$

and the $C2M$ is the inverse operator of $M2C$, which convert the column vector in equation (47) back to matrix M.

B. Proof of equation (35)

Proof:

$$\begin{aligned} &\left\| C2M(\mathcal{R}u^i_{a,k}) - H_{a,k+1}Y_a \right\| \\ =&\left\| C2M(\mathcal{R}u^i_{a,k}) - C2M(\mathcal{R}u^i_{a,k}) \cdot Y_a^+ Y_a \right\| \\ =&\left\| C2M(\mathcal{R}u^i_{a,k})(I - Y_a^+ Y_a) \right\| \end{aligned} \tag{48}$$

For any matrices Υ and A, $\|I - \Upsilon^+\Upsilon\| < \|I - A^+\Upsilon\|$ is always satisfied unless $\Upsilon = A$ [39], so

$$\begin{aligned} &\left\| C2M(\mathcal{R}u^i_{a,k}) - H_{a,k+1}Y_a \right\| \\ \leqslant&\left\| C2M(\mathcal{R}u^i_{a,k})\Big(I - C2M(\mathcal{R}u^i_{a,k})^+ C2M(\mathcal{R}u^i_{a,k-1})Y_a^+ Y_a\Big) \right\| \\ =&\left\| C2M(\mathcal{R}u^i_{a,k}) - C2M(\mathcal{R}u^i_{a,k-1})Y_a^+ Y_a \right\| \\ =&\left\| C2M(\mathcal{R}u^i_{a,k}) - H_{a,k}Y_a) \right\| \end{aligned} \tag{49}$$

■

C. Proof of equation (36)

Proof:

$$\begin{aligned} &\left\| \mathcal{R}u^i_{a,k} - M2C(H_{a,k}Y_a) \right\| \\ =&\left\| RR^+ M2C(H_{a,k}Y_a) - M2C(H_{a,k}Y_a) \right\| \\ =&\left\| (RR^+ - I)M2C(H_{a,k}Y_a) \right\| \end{aligned} \tag{50}$$

Similar to equation (49), we can have

$$\begin{aligned} &\left\| \mathcal{R}u^i_{a,k} - M2C(H_{a,k}Y_a) \right\| \\ \leqslant&\left\| \Big(RR^+ M2C(H_{a,k-1}Y_a) M2C(H_{a,k}Y_a)^+ - I \Big) M2C(H_{a,k}Y_a) \right\| \\ =&\left\| RR^+ M2C(H_{a,k-1}Y_a) - M2C(H_{a,k}Y_a) \right\| \\ =&\left\| \mathcal{R}u^i_{a,k-1} - M2C(H_{a,k}Y_a) \right\| \end{aligned} \tag{51}$$

■

D. Definition of Int operator

Given the estimated combined bias $\hat{B}_g$ and any H_g, for any gyroscope reading $y_g^{j,l}, (l = 1, 2, \cdots, N_j)$, we can have:

$$u_g^{j,l} = H_g(y_g^{j,l} - \hat{B}_g). \tag{52}$$

For any $u_g^{j,l}$, we can have the following Δq_l as

$$\Delta q_l = \begin{bmatrix} \frac{u_g^{j,l}}{|u_g^{j,l}|} \sin(\frac{|u_g^{j,l}|}{2}\Delta t) \\ \cos(\frac{|u_g^{j,l}|}{2}\Delta t) \end{bmatrix} \tag{53}$$

where Δt is the sampling interval. The quaternion q_j^l has the following property:

$$q_j^l = q_j^{l-1} \otimes \Delta q_l \tag{54}$$

where $\otimes$ is the quaternion multiplication and $q_j^0 = [0,\ 0,\ 0,\ 1]^T$. The $Int(y_g^{j,1:N_j}, H_g)$ can then be defined as:

$$Int(y_g^{j,1:N_j}, H_g) = q_j^{N_j}. \tag{55}$$

REFERENCES

[1] Z. Zhang, L.-Y. Ji, Z.-P. Huang, and J.-K. Wu, "Adaptive information fusion for human upper limb movement estimation," *Systems, Man and Cybernetics, Part A: Systems and Humans, IEEE Transactions on*, vol. 42, no. 5, pp. 1100–1108, 2012.

[2] B. Wang, Z. Deng, C. Liu, Y. Xia, and M. Fu, "Estimation of information sharing error by dynamic deformation between inertial navigation systems," *Industrial Electronics, IEEE Transactions on*, vol. 61, no. 4, pp. 2015–2023, April 2014.

[3] Z. Zhang, A. Panousopoulou, and G.-Z. Yang, "Wearable sensor integration and bio-motion capture: A practical perspective," in *Body Sensor Networks*. Springer, 2014, pp. 495–526.

[4] W. Wang and G. Xie, "Online high-precision probabilistic localization of robotic fish using visual and inertial cues," *Industrial Electronics, IEEE Transactions on*, vol. PP, no. 99, pp. 1–1, 2014.

[5] Z.-Q. Zhang and J.-K. Wu, "A novel hierarchical information fusion method for three-dimensional upper limb motion estimation," *Instrumentation and Measurement, IEEE Transactions on*, vol. 60, no. 11, pp. 3709–3719, 2011.

[6] H. Fourati, N. Manamanni, L. Afilal, and Y. Handrich, "Complementary observer for body segments motion capturing by inertial and magnetic sensors," *IEEE/ASME Transactions on Mechatronics*, vol. 19, no. 1, pp. 149–157, Feb 2014.

[7] Z. Zhang and X. Meng, "Use of an inertial/magnetic sensor module for pedestrian tracking during normal walking," *Instrumentation and Measurement, IEEE Transactions on*, vol. PP, no. 99, pp. 1–1, 2014.

[8] K. Sebesta and N. Boizot, "A real-time adaptive high-gain EKF, applied to a quadcopter inertial navigation system," *Industrial Electronics, IEEE Transactions on*, vol. 61, no. 1, pp. 495–503, Jan 2014.

[9] X. Meng, Z. Zhang, J.-K. Wu, W.-C. Wong, and H. Yu, "Self-contained pedestrian tracking during normal walking using an inertial/magnetic sensor module," *Biomedical Engineering, IEEE Transactions on*, vol. 61, no. 3, pp. 892–899, March 2014.

[10] J. Lötters, J. Schipper, P. Veltink, W. Olthuis, and P. Bergveld, "Procedure for in-use calibration of triaxial accelerometers in medical applications," *Sensors and Actuators A: Physical*, vol. 68, no. 1-3, pp. 221–228, 1998.

[11] A. Kim and M. Golnaraghi, "Initial calibration of an inertial measurement unit using an optical position tracking system," in *Position Location and Navigation Symposium, 2004. PLANS 2004*. IEEE, 2004, pp. 96–101.

[12] R. Zhu and Z. Zhou, "Calibration of three-dimensional integrated sensors for improved system accuracy," *Sensors and Actuators A: Physical*, vol. 127, no. 2, pp. 340–344, 2006.

[13] I. Skog and P. Händel, "Calibration of a mems inertial measurement unit," in *XVII IMEKO World Congress on Metrology for a Sustainable Development, September*. Citeseer, 2006, pp. 17–22.

[14] W. Li, Q. Du, and P. Mi, "A mems inertial sensor and amr magnetic sensor calibration method," in *Information, Communications and Signal Processing (ICICS) 2011 8th International Conference on*. IEEE, 2011, pp. 1–5.

[15] J. Skaloud, S. Guerrier, R. Molinari, M.-P. Victoria-Feser, *et al.*, "An algorithm for automatic inertial sensor calibration," in *Proceedings of ION GNSS+*, no. EPFL-CONF-188672, 2013.

[16] Z. Zhang and G.-Z. Yang, "Calibration of miniature inertial and magnetic sensor units for robust attitude estimation," *Instrumentation and Measurement, IEEE Transactions on*, vol. 63, no. 3, pp. 711–718, March 2014.

[17] V. Renaudin, M. H. Afzal, and G. Lachapelle, "Complete triaxis magnetometer calibration in the magnetic domain," *Journal of Sensors*, vol. 2010, 2010.

[18] J. Vasconcelos, G. Elkaim, C. Silvestre, P. Oliveira, and B. Cardeira, "Geometric approach to strapdown magnetometer calibration in sensor frame," *Aerospace and Electronic Systems, IEEE Transactions on*, vol. 47, no. 2, pp. 1293–1306, 2011.

[19] Z. Wu, Y. Wu, X. Hu, and M. Wu, "Calibration of three-axis magnetometer using stretching particle swarm optimization algorithm," *Instrumentation and Measurement, IEEE Transactions on*, vol. 62, no. 2, pp. 281–292, 2013.

[20] J. C. Springmann and J. W. Cutler, "Attitude-independent magnetometer calibration with time-varying bias," *Journal of Guidance, Control, and Dynamics*, vol. 35, no. 4, pp. 1080–1088, 2012.

[21] H. Pang, Q. Zhang, W. Wang, J. Wang, J. Li, S. Luo, C. Wan, D. Chen, M. Pan, and F. Luo, "Calibration of three-axis magnetometers with differential evolution algorithm," *Journal of Magnetism and Magnetic Materials*, vol. 346, pp. 5–10, 2013.

[22] Z.-Q. Zhang and G.-Z. Yang, "Micro magnetometer calibration for accurate orientation estimation," *Biomedical Engineering, IEEE Transactions on*, vol. PP, no. 99, pp. 1–1, 2014.

[23] A. Fitzgibbon, M. Pilu, and R. Fisher, "Direct least square fitting of ellipses," *Pattern Analysis and Machine Intelligence, IEEE Transactions on*, vol. 21, no. 5, pp. 476–480, 1999.

[24] I. Markovsky, A. Kukush, and S. Huffel, "Consistent least squares fitting of ellipsoids," *Numerische Mathematik*, vol. 98, no. 1, pp. 177–194, 2004.

[25] Q. Li and J. G. Griffiths, "Least squares ellipsoid specific fitting," *Geometric Modeling and Processing*, vol. 0, p. 335, 2004.

[26] N. Chernov and H. Ma, "Least squares fitting of quadratic curves and surfaces," *Computer Vision*, pp. 285–302, 2011.

[27] A. S. Nemirovski and M. J. Todd, "Interior-point methods for optimization," *Acta Numerica*, vol. 17, pp. 191–234, 2008.

[28] W. W. Hager and H. Zhang, "A new active set algorithm for box constrained optimization," *SIAM Journal on Optimization*, vol. 17, no. 2, pp. 526–557, 2006.

[29] J. Nocedal and W. S. J., *Numerical Optimization, Second Edition.* Springer Series in Operations Research, Springer Verlag, 2006.

[30] M. H. Loke and R. Barker, "Rapid least-squares inversion of apparent resistivity pseudosections by a quasi-newton method," *Geophysical prospecting*, vol. 44, no. 1, pp. 131–152, 1996.

[31] J. C. Lagarias, J. A. Reeds, M. H. Wright, and P. E. Wright, "Convergence properties of the nelder–mead simplex method in low dimensions," *SIAM Journal on Optimization*, vol. 9, no. 1, pp. 112–147, 1998.

[32] F. Sun, X. Hu, Y. Zou, and S. Li, "Adaptive unscented kalman filtering for state of charge estimation of a lithium-ion battery for electric vehicles," *Energy*, vol. 36, no. 5, pp. 3531–3540, 2011.

[33] B. Lo and G. Yang, "Key technical challenges and current implementations of body sensor network," in *Proc. 2nd International Workshop on Body Sensor Networks (BSN 2005)*, 2005.

[34] Analog Devices ADXL330. [Online]. Available: http://www.analog.com/en/sensors/inertial-sensors/adxl330/products/product.html

[35] Invensense ITG-3200. [Online]. Available: http://invensense.com/mems/gyro/itg3200.html

[36] Honeywell HMC5483. [Online]. Available: www.magneticsensors.com/datasheets/HMC5843.pdf

[37] BTSBioengineering. [Online]. Available: http://www.btsbioengineering.com/

[38] Z.-Q. Zhang, X.-L. Meng, and J.-K. Wu, "Quaternion-based kalman filter with vector selection for accurate orientation tracking," *Instrumentation and Measurement, IEEE Transactions on*, vol. 61, no. 10, pp. 2817–2824, 2012.

[39] C. B. Moler, "Least squares," in *Numerical Computing with Matlab*. Society for Industrial and Applied Mathematics, 2004, ch. 5, pp. 139–163.

Zhi-Qiang Zhang received the B.E. degree in computer science and technology from School of Electrical Information and Engineering, Tianjian University, China, in 2005, and the Ph.D. degree from the Sensor Network and Application Research Center, Graduate University, Chinese Academy of Sciences, Beijing, China, in 2010.

He is currently a Research Associate with the Hamlyn Centre for Robotic Surgery, Department of Computing, Imperial College, London. His research interests include Body Sensor Network, Information Fusion, Machine Learning and Targets Tracking.